Serving the grease industry since 1933

NLGI

India Chapter

ISSN : 0972-2742

GREASETECH INDIA

A Quarterly Journal of NLGI-India Chapter

Vol. XIX, No. 3, Jan - March 17

GREASETECH INDIA

A Quartely Journal of NLGI-India Chapter

Vol. XIX, No. 3, Jan - March 17

In This Issue Page No

1. Blends; Friend or Foe? Base Oil Blends for Grease Formulations 3-10
2. Base Oil Classification Using Principle Component Analysis And Mid / Near Ir Spectroscopy 11-16
3. Stability and thermal conductivity of graphene nanolubricants 17-33

Blends; Friend or Foe?
Base Oil Blends for Grease Formulations

Mehdi Fathi-Najafi Senior Technical Coordinator
Nynas AB

Abstract

Mineral oils used by grease manufacturers can be divided into two major groups, naphthenic oils and paraffinic oils. These categories of base oils have their own advantages and disadvantages depending on the applications and conditions. The most important advantages of the naphthenic oils over the paraffinic oils, with the same viscosity and similar aromatic content, are better low-temperature flowability and better solvency.

The contribution of having base oils with good solvency towards the thickener is that less thickener is needed to obtain a certain consistency of the finished product. For instance, a typical NLGI grade 2 lithium based grease, based on a solvent neutral 500, Gr I oil, may contain 10-14 wt% thickener; while 6- 8% thickener is required for an equivalent viscosity oil of naphthenic nature.

Using blends of naphthenic oil and paraffinic group one oil (Gr I) have successfully been used during the recent years in India. However, the author believes that the surplus of paraffinic Gr II and Gr III base oils is one among a number of market trends that brings some great opportunities to the grease formulators, if they look for blends where naphthenic oils are regarded as part of the solution for a sustainable formulation. A number of key parameters important for the performance of the finished product could be obtained within reasonable cost.

The purpose of this work was to compare "side by side" three base oil blends where paraffinic Gr I, Gr II and Gr III, in combination with naphthenic, were used for preparation of lubricating greases.

The overall results, obtained in this study, reveal some interesting aspects of the use of paraffinic Gr II as a substitute to paraffinic Gr I for preparation of greases. The outcome of this work emphasizes that

a) blends should be regarded as a great opportunity for grease formulators who are looking for some further development of their current formulations and furthermore, and
b) the lubricating grease based on the blend of paraffinic Gr II and naphthenic oil performs better than others.

Key words: traction coefficient, low temperature flowability, oxidation stability. elastomer compatibility, Thickener content, naphthenic oil, paraffinic oil, lithium based grease

Preparation and Characterization of the Base Oils

The target for this study was to compare different oil mixtures, where the main focus was on the possible synergies of the blends between paraffinic oils and naphthenic oil. For this reason, three base oil blends have been prepared by using three paraffinic base oils, representing Gr I, Gr II and Gr III, with one naphthenic oil. Table 1 displays the typical characteristics of the three paraffinic base oils and the naphthenic oil.

Properties	Unit	Method (ASTM)	**Gr I**	**Gr II**	**Gr III**	**Gr V**
Type of oils			Paraffinic	Paraffinic	Paraffinic	Naphthenic
Viscosity at 40 ºC	mm^2/s	D 445	90	110	49	440
Viscosity at 100 ºC	mm^2/s	D 445	10.1	11.9	7.9	19.9
Viscosity index	-	D 2270	95	97	130	19
Density at 15 ºC	kg/m^3	D 4052	888	875	820	931
Flash point	ºC	D 93A	260	269	261	221
Pour point	ºC	D 97	-12	-15	-12	-12
Aniline point	ºC	D 611	99	124	117	88

Table 1: Typical characteristics of the paraffinic base oils.

As it can be seen in Table 1, the paraffinic oils had different viscosities at 40 (ºC); subsequently different wt % of the naphthenic oil was used to obtain 150 (mm^2/s) in viscosity at 40 (ºC). The characterizations of the base oil blends cover a wide range of tests. Table 2 shows the characteristics of these three base oil blends that have been used for preparation of greases.

Properties	Unit	Method (ASTM)	**Blend A**	**Blend B**	**Blend C**
Viscosity at 40 ºC	mm^2/s	D 445	147	149	148
Viscosity at 100 ºC	mm^2/s	D 445	12.4	13.4	12.8
Viscosity index	-	D 2270	66	82	73
Density at 15 ºC	kg/m^3	D 4052	903.2	888.8	899.4
Reflective index at 20 ºC		D 1747	1.496	1.487	1.495
Flash point	ºC	D 93A	223	239	235
Pour point	ºC	D 97	-21	-24	-27
Aniline point	ºC	D 611	99.8	116.0	104.3
Total acid number	mg KOH/g	D 974	0.017	0.012	0.021
Copper strip test		D 130	1a	1a	1a
Carbon type composition	wt %	D 2140			
C_A			9.0	3.2	7.5
C_P			58.6	64.6	66.4
C_N			32.1	32.4	21.6

Table 2: Characteristics of the base oil blends.

Table 2 reveals that although the viscosity of the blends at 100 ºC varies within 1 mm^2/s, but there is a bigger gap between the viscosity indexes which a result of two parameters; the starting viscosity index of the oils and the percentage of the naphthenic oil involved. Further impact of the naphthenic oil on the blends can be noted in the parameters such as aniline point and pour point.

Tribological Measurements of the Base oil Blends

A mini traction machine (MTM2, PCS Instruments) has been used to measure the frictional properties of the base oil blends in a mixed rolling/sliding contact.

A load is applied to a steel ball, and with a force transducer the frictional force is measured as the ball is in contact with a steel disc. The Slide to Roll Ratio (SRR) is defined as the percentage ratio between the sliding speed (difference between the ball speed and the disc speed) and the mean speed. Consequently, 0 % is pure rolling and 200 % is pure sliding. Furthermore, by measuring the traction (friction) as a function of the mean speed at constant SRR, a Stribeck curve can be obtained.

In this study, the friction measurements were performed in a steel/steel contact at 820 MPa and a steel ball with a diameter of 19.05 mm (3/4") was used. Both the steel ball and the steel disc where made of AISI 52100 steel and had a smooth finish with a roughness less than 0.01 µm (Ra). Four consecutive runs were measured, and the mean value of the measurements is displayed. Two tests for each base oil blend were performed and very good agreement was observed for the tests. The temperature was kept constant at 40 ºC for all MTM measurements.
A Stribeck curve was obtained by measuring the Traction coefficient of the blends as a function of speed at constant SRR (50%), see Figure 1. This figure indicates slightly lower traction coefficient for blend B.

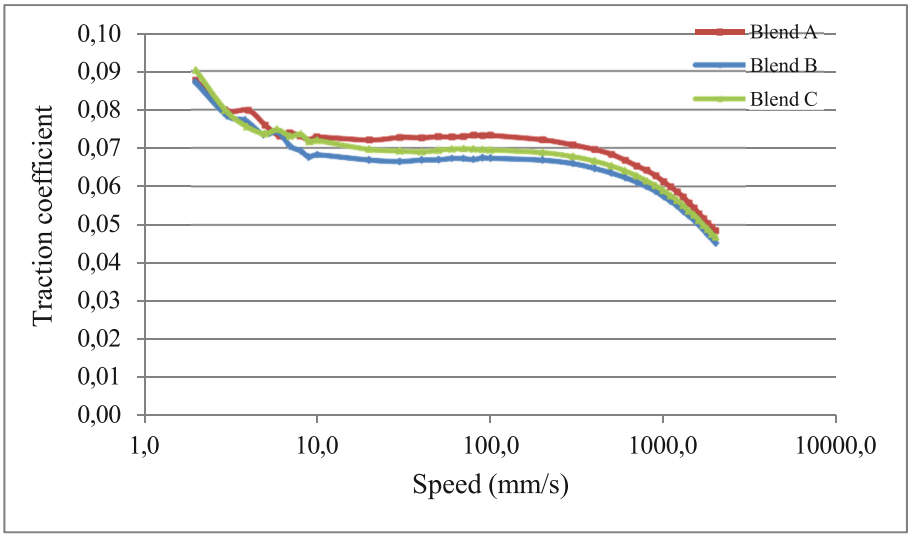

Figure 1: Traction coefficient as a function of speed, measured at 40 ºC

Electrical Contact Resistance (ERC): ERC describes the degree of separation between the Ball and the Disc in a MTM. Hence, when they are fully separated from each other the voltage at the disc will be the same as the applied one (15 V) and if they are fully separated (100%) e.g. by base oil, then the balance resistor will be 0 V.

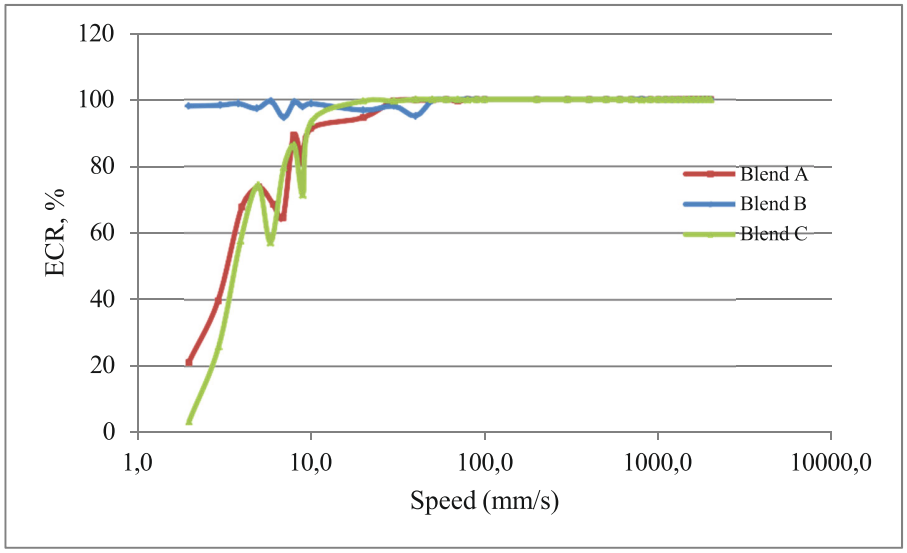

Figure 2: Effect of Speed on ECR measurements.

Based on the measured ECR, at different speeds, for the three blends, see Figure 2, a better performance for the Blend B at lower speeds can be observed. This measurement reveals that the film thickness of Blend A and C are reduced significantly at lower speeds. However, based on these few measurements, it is not understood why Blend B contributes to more stable film thickness regardless the speed.

Preparation and Characterization of the Greases

The three base oil blends (A, B and C) have been used for preparation of lithium based greases in an open kettle where lithium hydroxide was reacted with 12-hydroxy stearic acid. Greases A, B and C were made with base oil blends A, B and C respectively. Notable that no additive was used in these greases.

In order to make the comparison easier, each blend was used during the entire production of the grease, meaning a blend was used in both cooking and cooling stages.

Characteristics of the greases	Unit	Method ASTM	Grease A	Grease B	Grease C
Base oil type (naph+para)			Blend A	Blend B	Blend C
Penetration (0)	mm^{-1}	D 217	281	289	283
Penetration (60 str)	mm^{-1}	D 217	280	287	284
Penetration (10^5 str)	mm^{-1}	D 217	296	293	298
Diff in penetration after 10^5 str			+16	+6	+12
Dropping point	ºC	IP 396	202	200	203
Soap content	wt %		8,23	8,83	6.39
Wear scar (400N / 60 min)	mm	DIN 51350:5	0.86	0.89	1.00
Cu-corrosion		D 4048	1b	1b	1b
Texture			Smooth & Buttery	Smooth & Buttery	Smooth & Buttery

Table 3: The characteristics of the Greases

Based on the obtained results shown in Table 3, some conclusions may be drawn such as:

- a low soap content in Grease C was needed to achieve the penetration target, probably due to a higher wt % of naphthenic oil involved.
- good shear stability was achieved for all three greases were obtained.
- the slightly higher wear scar resulted by Grease C probably can be explained by its lower thickener content. The measured wear scars for all three greases are in-line within the expected wear scar for a neat lithium based grease.

Elastomer Compatibility

Chloroprene rubber is one of the most common elastomers used in constant velocity joints application. Hence, the rubber interactions with the lithium grease, based on the three Blends, were conducted through total immersion of the rubber sample in the greases. The test duration was 168 hours at 100 ºC.

The change in hardness and weight of the chloroprene rubber samples was measured. Hardness is a measurement of a rubber's ability to resist penetration of a specified metal rod with a specifically shaped tip or end. In order to measure the change in hardness of the rubber, the IRHD (International Rubber Hardness Degrees) method was used.

Previous publications have shown that the Aniline point of the oil has significant influence on the interaction between the oil, the corresponding grease and the rubber. For example, in the case of Nitrile butadiene rubber, an oil with low aniline point is recommended, while high aniline point is desired for Chloroprene rubber. This part of the work confirms that recommendation. Base oil Blend B, used for

Grease B, has the highest aniline point (116 ºC), and this is reflected in the obtained results, see Figures 5 and 6.

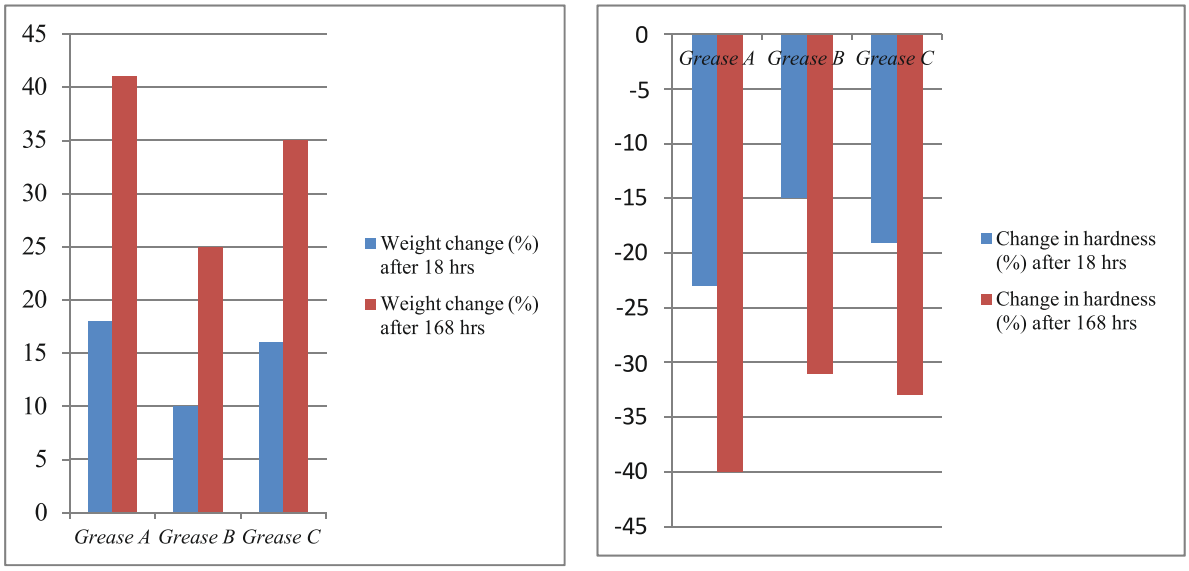

Figure 3: and 4: show the impact of different greases on C.R. after various times at 100 ºC

.

Oxidation Stability Tests

The standard oxidation stability test according to ASTM D 942, also called rotary bomb test (Norma- Hoffman), has been used. The obtained results, pressure drop, for all three greases were 2 psi which is regarded to be very good despite of the fact that the greases do not contain any antioxidant.

At the last ELGI annual meeting a new oxidation test method for measuring oxidation stability of lubricating grease was introduced by George Dodoes [0]. The suggest method, RSSOT (The Rapid Small Scale Oxidation Test) has been described as a more reliable and faster test for determination of the oxidation stability of lubricating greases. This test is frequently used for measurement of the resistance of various types of fuels (ASTM D 7545). Figure 3 and 4 show the photo of these two test apparatuses respectively.

Figure 5: Rotary bomb test apparatus

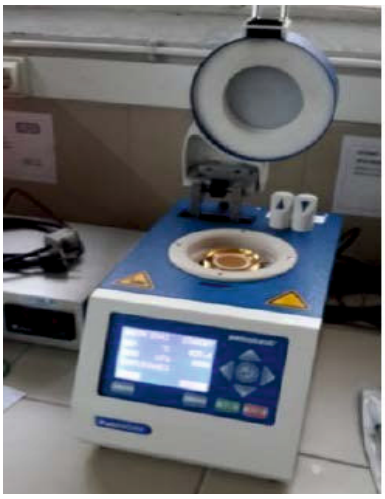

Figure 6: RSSOT apparatus

According to this method, a breakpoint at with a pressure drop of 10% below the initial applied oxygen pressure (preferably at 700 kPa) is recorded as the induction time at a constant temperature. In order to be able to compare the obtained results for these three greases with the published data, it was decided to carry the tests with the following condition: the applied temperature and Pressure has been kept constant at 140 ℃ and 700 kPa respectively. Table 4 shows the average induction time obtained for the three samples after two runs.

Samples	Induction Time (min)		
	1st Measurements	2nd Measurements	Mean value
Grease A	499	497	498
Grease B	828	819	824
Grease C	597	573	585

Table 4: Induction time for Greases at 140 ℃

As it can be seen, RSSOT test reveals a variation between the samples. Grease B (Gr II + naphthenic) > Grease C (Gr III + naphthenic) > Grease A (Gr I + naphthenic). Notable that, according to published data by other authors, fully formulated lithium based grease with similar viscosity has shown to have an induction time of less than 200 min at the same condition.

Flow Pressure Measurements

In order to simulate the pumpability of the greases, the flow pressure (FP) of the greases at two different temperatures (-20 ºC and -35 ºC) have been measured, according to DIN 51805. The test setup consists of a conical nozzle that is filled with grease. The nozzle is placed in the measuring instrument, equilibrated for 2-3 hours at a desired temperature, and then an increasing

pressure is applied to the nozzle. The threshold pressure at which grease starts to flow through the nozzle is recorded.

Characteristics	Pour point of the base oil Blends (ºC)	FP (mbar), at -20 ºC	FP (mbar), at -35 ºC
Grease A	-21	350	1100
Grease B	-24	300	700
Grease C	-27	200	525

Table 5: The impact of temperature on the base oil blends (PP) and the corresponded greases (FP)

Flow pressure measurements show very good low temperature properties for the Greases. However, Grease C (Gr III + Naphthenic Oil) shows superior low temperature behaviour, followed by Grease B (Gr II + Naphthenic oil), when compared with Grease A (Gr I + Naphthenic).
If the flow pressure for the Greases measured at – 20 ℃ are compared with each other it will be found that the differences cannot be explained by the pour point of the base oil blends which is quite interesting. Therefore, in-line with previous finding, using pour point of the base oil in order to predict the flowability of a lubricant could be regarded as a misinterpretation.

Summary

Three base oil blends have been prepared by using a high viscous naphthenic oil and three paraffinic oils, one from each group (Gr I, Gr II and Gr III). The characterization of the blends emphasizes that all three blends have similar properties. However, the thermal stability test which is in fact a static test, and MTM measurements, indicate slightly better performance for Blend B, which contains paraffinic Gr II oil.

The three lithium based greases, which are corresponding with the three base oil blends, show good performance in a number of tests. In the rubber compatibility test, Blend B shows less impact, and therefore should be regarded as a better candidate. Regarding the low temperature behavior of the greases, Grease C seems to be a better product.
This study emphasizes the potential of taking advantage of the ongoing fundamental change within the base oil industry, which has created, and will continue to create, new opportunities to upgrade the current (old) grease formulations, by using blends of paraffinic oils, preferably Gr II, and naphthenic oil.

Acknowledgment

The Author is grateful to the following companies who contributed with the oxidation stability measurements; Standard Greases (India) with Rotary “bomb” test and Eldon´s S. A. (Greece) with RSSOT.
Last but not least, the author is thankful the co-workers at Nynas; Linda Malm, René Abrahams and Luis Bastardo-Zambrano for their contributions to this study.

Reference

[1] Salomonsson, L., et. al, Oil/Thickener interaction of chloroprene and nitrile-butadiene rubber with lubricating greases and base oil. Lubricating oil, 2006. 21(54)
[2] Serra-Holm V., Development of a novel naphthenic base oil for application in CVJ greases, NLGI 73rd Annual Meeting, October 2006, FL (US).

[3] Sullivan, T., Tighter base oil supply expected in Europe. Lube report 2012.

[4] Fathi-Najafi, M., et al., Low temperature tribology. A study of the influence of base oil characteristics on friction behaviour under low temperature conditions. EUROGREASE, 2012
.
[5] Bastardo-Zambrano L. Fathi-Najafi, M., Base oil blends to meet the new demands of the lubricant industry, Lubes Magazine No.115 June 2013.

[6] Fathi-Najafi M. et.al, When the going gets tough... A heavy specialty oil for grease formulations (Part II), NLGI Spokesman November/December 2014, Vol. 78 (No5).

[7] Dodoes, G. S., A new approach for measuring oxidation stability of
lubricating greases, ELGI 26rd Annual Meeting (Croatia), 2014.

[8] http://www.pcs-instruments.com/mtm/accessories/mtm-cr.shtml#page=page-1

Base Oil Classification Using Principle Component Analysis And Mid / Near Ir Spectroscopy

E. Ramu*, Veena Bansal, Ratnadeep S Joshi, V Kagdiyal, A A Gupta
Research & Development Center

Abstract:

Mid- IR (MIR) spectroscopy is commonly used spectroscopic technique for theidentification of Mineral (Gr I-III), Parafinic, Naphthenic, Heavy Alkylated Benzenes (HAB), Low Alkylated Benzenes (LAB) base oils due to characteristic features at ~3000-3100 (aromatic CH stretching), 1600 (aromatic ring vibrations) and 600-800 cm^{-1}(aromatic CH bending & wagging). Parafinic base oils show similar features like Gr I-III except in aromatic region. Group IV base oils like Poly-α-olefins (PAO) exhibits similar features as those of Gr I-III and Parafinic base oils but differs in peak height at 722 cm^{-1}. Since Near IR (NIR) region covers the overtone and combination bands, the differences in spectral features for different base oils are not significant.
The present study adopted to understand the use of Principle Component Analysis (PCA) to overcome the draw backs of MIR / NIR raw spectra in distinguishing the different base oil types (Mineral, PAO, HAB, LAB), in particular PAO from mineral type base oils. PCA is applied on raw spectra, 1st derivative and 2nd derivative spectrum generated from the MIR and NIR spectroscopic techniques. PCA results (Score plots) are self-explanatory in understanding the objective of the study. From the results, first two principle components extract more variance from 2nd derivative spectrum (94 and 91% for MIR and NIR respectively) than the raw and 1st derivative spectrum. Score plots show the five different classes of base oil groups, Class 1: Gr I- III, Class 2: Parafins - Naphthenes, Class 3: HAB, Class 4: LAB, Class 5: PAO. This study demonstrates the strength of PCA to evaluate the spectral data critically and extracts the valuableinformation where both MIR and NIR raw data fails to explain. Current methodology has been found easy to transfer or to use in Quality Control (QC) labs for ready identification of base oil types for their subsequent use in product development of greases, gear oils and other lubricants.

Key words: Base oils, Mineral oil, Low Alkylated Benzenes, Heavy Alkylated Benzenes,Poly-alfaolefins, Principle component analysis, Scores plot.

1.0w Introduction: Lubricants viz Grease and Gear oils composed of base oil as a major component and careful selection of the same plays vital role in its performance. Base oils used for formulating the grease and gear oils are classified into several types based on their source viz.Gr I - III, Gr – IV (polyalfaolefins), Gr - V (other than Gr I – IV). Gr I – III base oils are also called as mineral based as these are distillates of crude oil. The differentiation of Gr I – III base oils are done based on components like saturates, aromatics, sulfur and physical property like Viscosity Index. The optimum composition of the Base oil with reference to saturates, aromatics and Naphthenic are

necessary to achieve the required performance of the final lubricant formulation. PCA treat the spectroscopic data on the basis of sample types and its correlation to spectroscopic data given. Samples are initially projected onto the hundreds to thousands in number of variables (wavelength) space which is difficult to understand. PCA generates the significantly less number of principle components (maximum of five) to understand the spectral variability for all the samples under study hence it can be called as data reduction technique. The advancement of computers made it easy to perform the PCA analysis on spectroscopic data usingthe commercially available software. Determination of type of base oils prior to the lubricant development process is a primary job to analytical scientist. MIR spectroscopy is a commonly used to technique to classify the base oils where as it fails to distinguish PAO from Gr I-III and paraffinic base oils. NMR will be helpful to overcome the difficulties in MIR spectroscopy but it is not suitable to apply in quality control laboratories. Use of PCA on spectroscopic data to draw qualitative and quantitative aspects of crude oil [1], mineral – vegetable base oils [2-9], Diesel [10], lubricants [11-13]. Multivariate analysis on infrared spectroscopic data is well documented in ASTM standard E1655 [14]. In the present paper, use of PCA to distinguish the base oils viz Gr I-III, Parafinic, Naphthenic, PAO, LAB, HAB is demonstrated.

Fig 1: Mid IR (4000-400cm^{-1}) & Near IR (6200-4000cm^{-1}) spectra of Base oils

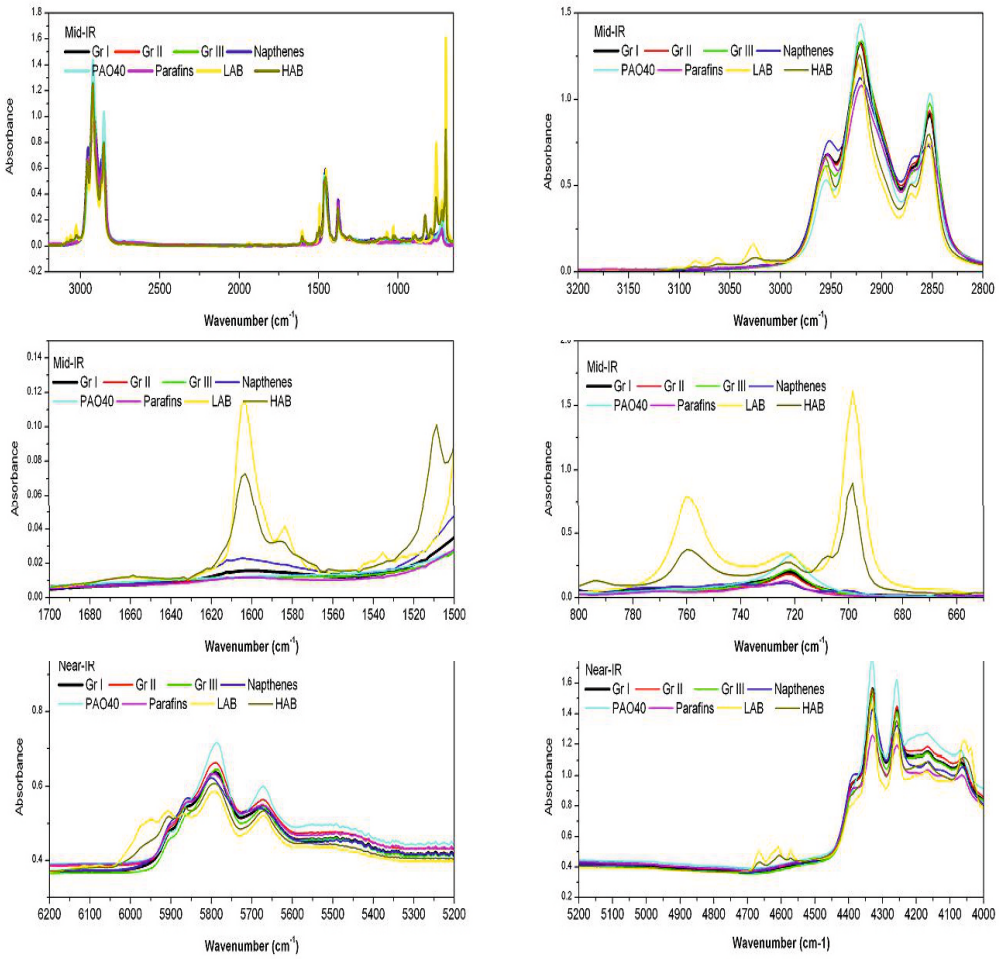

2.0 Materials and Methods: Twenty seven commercial base oils samples: Gr I (5 no's), Gr II (4 no's), Gr III (2 no's), Polyalfaolefins (5 no's), LAB (2 no's), HAB (2 no's), Parafinic (1 no's), Naphthenic (6 no's) are selected for the study. MIR (FT-IR spectrometer, IRPrestige-21, Shimadzu Corp.) analysis of base oils is recorded using the acquisition parameters: scan range - 4000-650 cm^{-1}, resolution – 4 cm^{-1}, no. of scans - 50. NIR (Near – IR Spectrometer, Frontier, PerkinElmer Inc.) analysis performed on base oils using the acquisition parameters: scan range 10000-4000 cm^{-1}, resolution – 4 cm^{-1}, no. of scans - 32.

Fig 2: Mid & Near IR 1st & 2nd order Derivative spectra of Base oils

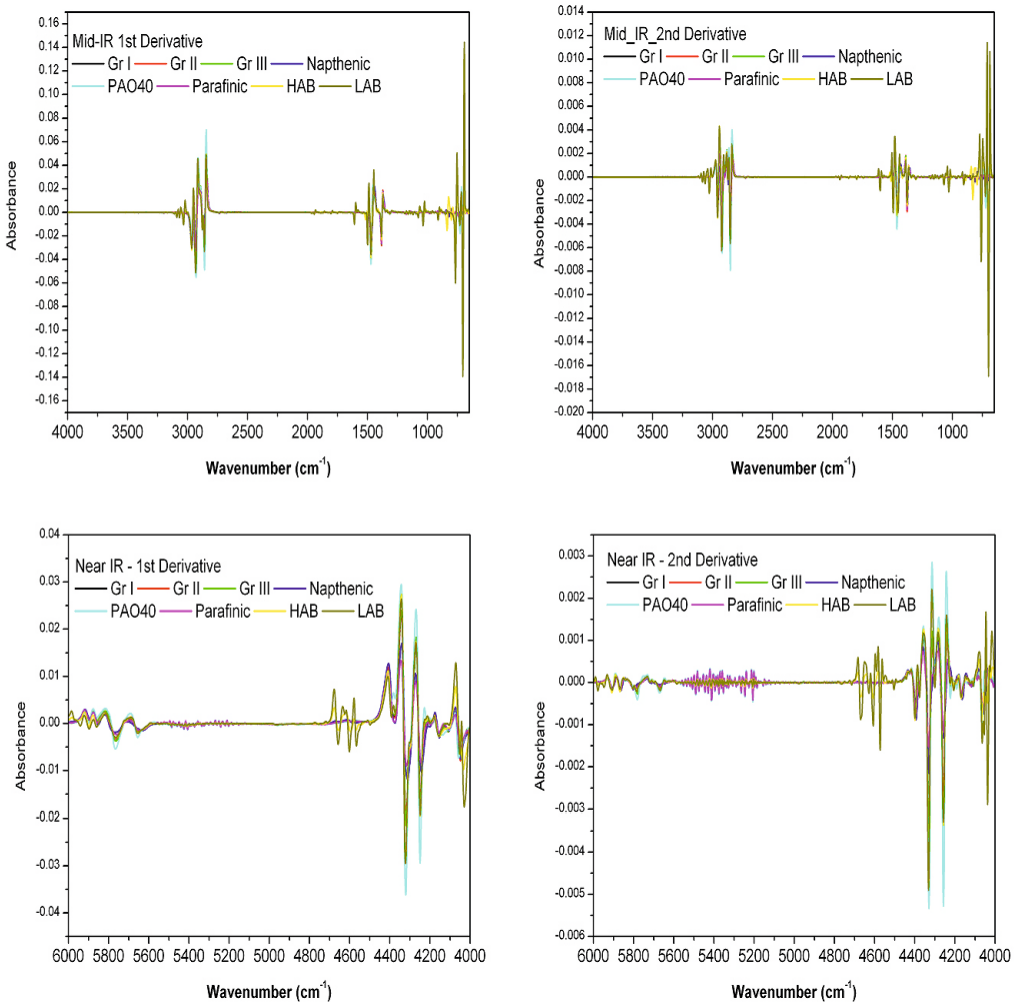

3.0 Experimental: Sampling method chosen for the MIR and NIR analysis is HATR accessory (10 bounce ZnSe window, PIKE Tech) and NIRA diffuse reflectance accessory (glass petri dish and aluminium back reflection plate). MIR & NIR spectra are imported to The Unscrambler® (Camo Software AS, Norway) for Principle Component Anlaysis (PCA) analysis. First and second order spectra are generated using Savitzky-Golay algorithm with 27 smooth points. PCA analysis is performed on mean centered raw, 1st derivative and 2nd derivative spectra of base oils with NI-PALS algorithm. Principle components chosen are five and the PCA model is validated using full cross validation method. Score plots for first two principal components are extracted for all the spectral in-put from the PCA software.

Fig 3: PCA Score Plots (PC1 vs PC2) generated from Mid & Near IR Spectra of Base oils

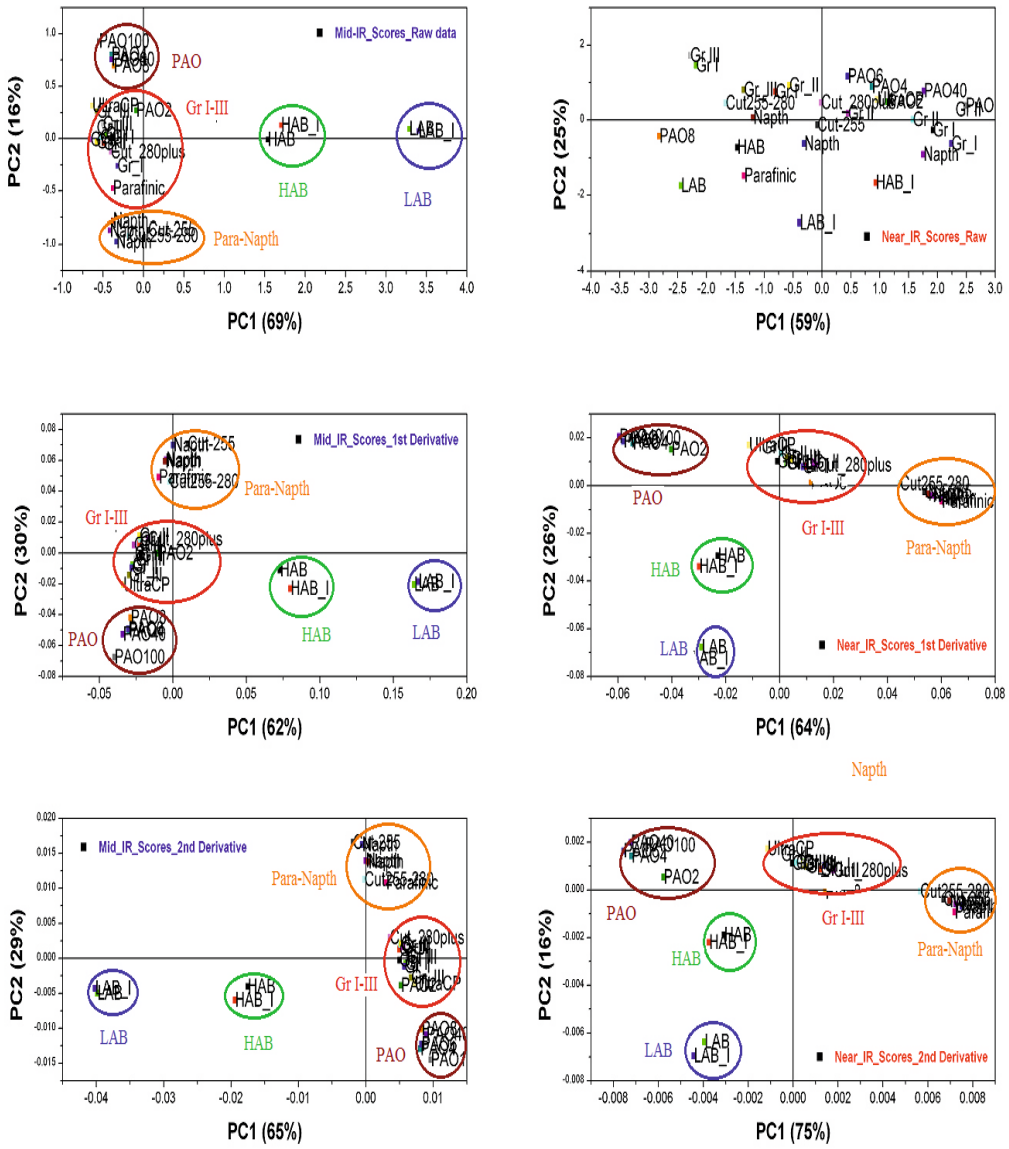

4.0 Results and Discussion: MIR spectra of base oils show the differences in the regions 3100-2800, 1650 – 1500 and 800-600cm^{-1} corresponds to –CH str (aromatic & aliphatic), -C=C- (aromatic ring vibrations), -CH bending (aromatic & aliphatic). Even the base oils as the name given as paraffinic or naphthenic, they will contains Naphthenic or paraffinic components in significant quantity respectively. As the Naphthenes are structural isomers of parafins, no significant differences are seen in the IR spectrum. LAB and HAB shows the high in aromatic and can be clearly distinguishable from the rest of the base oils. Due to differences in aromatic content, Gr I-III base oils can be differentiated using the peak around 1600cm^{-1}. Polyalfaolefins (PAO) is a polymer of alfaolefin (double bond is in between C_1 and C_2) provides viscous liquids rather forming crystalline solids from other olefin class. PAO is composed of CH_3, CH_2, and CH moieties in their structure, shows similar features like Gr III or paraffinic or naphthenic base oils except with intense peak at 722cm^{-1}(~2.5 times). MIR and NIR absorbance spectra and derivative counter parts are shown in Fig 1 & Fig 2. Score plots (Fig 3) shows MIR spectral variance explained by the first two principle components for raw, 1st derivative and 2nd derivativeare 69 (PC1), 16(PC2); 62(PC1), 30(PC2) and 65(PC1), 29(PC2) % respectively. Total explainedMIR spectral variance of first two principle components increases from raw (85%) to 1st order (92%) and followed by 2nd order derivative (94%). Score plots of MIR spectra shows five different classes in which raw spectra score plot shows the Parafinic base oil is with Gr I-III classwhere as 1st and 2nd derivative spectra shows paraffinic and Naphthenic base oils as one class. Rest of the base oils PAO, LAB and HAB are well separated from the Gr I-III, Parafinic - Naphthenic base oil classes. NIR spectral variance explained by the first two principle components for raw, 1st derivative and 2nd derivative are 59(PC1), 25(PC2); 64(PC1), 26(PC2); 75(PC1), 16(PC2) %. Total explained NIR spectral variance of first two principle components increases from raw (84%) to 1st order derivative (90%) and followed by 2nd order derivative (91%). Score plots (Fig 3) of 1st and 2nd derivative Near IR spectra shows five different classes: Class 1 Gr I-III class 2 Parafinic & Naphthenic, Class 3 PAO, Class 4 LAB and Class 5 HAB.

5.0 Conclusions: The present MIR and NIR technique coupled with PCA can able to distinguish the different base oil types used in formulating the grease and gear oils. Even though spectral variance explained by the PC1 and PC2 is significant (84%), random distribution of base oils in the score plots shows the weakness of the raw NIR spectra in distinguishing the base oil classes over 1st and 2nd order derivative spectra. Results show the higher order derivative spectra carry the more variance and are more effective in classification of base oils. MIR or NIR spectra are assuch fails to explain the spectral differences between the samples where the use of PCA along with spectroscopic data will become a powerful tool to see the minute changes between the samples. The distance between the spectroscopic data projected on the score plot is small; then the spectral variance between the samples is not significant and remains in same class. The present methodology is studied for commercially available base oils labeled as Gr I – III, Parafinic, Naphthenic, PAO, LAB and HAB. Applicability of the current protocol for the different base oil mixture is planned for future research.

6.0 References

1. Etukudo, Ifiok U., Okop, Imeh J. , Obadimu, Clement O. Discerning Group-Type Analysis of Crude Oils from Osso Platform, Nigeria, Using Vibrational Spectroscopy with Multivariate Statistics. Int. J. of Engg. and Sci. 3(6) 2014 p06-17
2. Olejniczak A, Chostenko A.G., Fall J. Discrimination of base oils and semi-products using principal component analysis and self organizing maps. Fuel 89(5) 2010 p1150-1155.
3. Julio Cesar Laurentino Alves*a and Ronei Jesus Poppia Determining the presence of aphthenic and vegetable oils in paraffin-based lubricant oils using near infrared spectroscopyand

support vector machines Anal. Methods, 5 (22) 2013, p6457-6464
4. Stella M. Rios, Mercedes Barquín, Norma Sbarbati Nudelman. Characterization of oil complex hydrocarbon mixtures by HSQC-NMR spectroscopy and PCA. J. Physical organic chemistry, 27 (4) 2014 p352-357.
5. F.S.G. Lima, M.A.S. Araújo, L.E.P. Borges. Determination of the carcinogenic potential of lubricant base oil using near infrared spectroscopy and chemometrics. Tribology International, 36 (9) 2003 p691–696.
6. Tomas Cajka, Katerina Riddellova, Eva Klimankova, Monika Cerna, Frantisek Pudil, Jana Hajslova. Traceability of olive oil based on volatiles pattern and multivariate analysis. Food Chemistry 121 (1) 2010 p282–289
7. M. Elbir, J. Oukrich, A. Moubarik, A. Amhoud, M. Fakir, M. Berkani, M. Naciri Bennani. M. Mbarki. Chemometric authentification of Moroccan Picholine virgin olive oil by automatic classification based on the composition of fatty acids and sterols. J. Mater. Environ. Sci. 5 (1) 2014 p101-110.
8. Rusak, David A.; Brown, Leah M.; Martin, Scott D. Classification of Vegetable Oils by Principal Component Analysis of FTIR Spectra. J. Chemical Education, 80 (5) 2013 p541
9. Suzana Ferreira-Dias, Dina G. Valente, José M.F. Abreu. Pattern recognition of acorns from different Quercus species based on oil content and fatty acid profile. Grasas y Aceites 54 (4) 2003 p384-391.
10. Guang Pu Xue Yu Guang Pu Fen Xi. Application of PCA to diesel engine oil spectrometric analysis PubMed commons, 30(3) 2010 p779-82
11. Xu, R. Nguyen, H. Sobol, P. Wang, S.L. Wu, A. Johnson, K.E. Application of principal component analysis to the FTIR spectra of disk lubricant to study lube-carbon interactions. IEEE Transactions on Magnetics 40(4) 2004 p3186-3188
12. Borin A, Poppi RJ. Multivariate Quality Control of Lubricating Oils Using Fourier Transform Infrared Spectroscopy. *J. Braz. Chem. Soc*. 15(4) 2004 p570-576
13. Dave Wooton, Robert Thomas, Stuart Barry. Using Infrared Spectroscopy in Used Engine Oils – Estimating Base Number. http://www.machinerylubrication.com/Read/808/infrared-spectroscopy-oil
14. Standard Practices for Infrared Multivariate Quantitative Analysis, American Society for Testing and Materials (ASTM) E1655.

Acknowledgements

The authors thank Management, Research & Development Center, Indian Oil CorporationLimited, for providing the facilities and permission to publish the work.

Stability and thermal conductivity of graphene nanolubricants

Abdul Khaliq Rasheed[1], Mohammad Khalid[1], Rashmi Walvekar[2], TCSM Gupta[3], T. Saritha[3]Andy Chan[1]

[1]Manufacturing & Industrial Processes Division, University of Nottingham Malaysia Campus,43500 Semenyih, Selangor, Malaysia.

[2]Department of Chemical Engineering, Taylor's University, Lakeside Campus, 47500 SubangJaya, Selangor, Malaysia

[3]Lube World Holdings Sdn. Bhd., Dataran Prima, Petaling Jaya,, Selangor, Malaysia

Abstract

Advancement in automotive sector and precision manufacturing industries demand efficient lubricants to overcome wear and losses due to poor heat transfer. Many nanoparticles have been found to have extreme pressure, anti-wear and thermal properties making them suitable as lubricant additives. In this research, we have investigated the effect of graphene flakes (60 nm thick) on the stability, thermal conductivity and tribology aspects of mineral oil based lubricants. The thermal conductivity of oil was found to increase upto 22.3% at 80°C with 0.01wt % of graphene. The enhancement depends on the graphene concentration (0.01-0.1 wt%), size (8 nm, 12 nm and 60 nm thick) and temperature (30-80°C). The as-synthesized graphene flakes were not stable in the mineral oil and therefore the thermal conductivity decreases over time. Nevertheless, the presence of dispersants in the oil formulation enhances the stability significantly. Graphene's size dependent thermal conductivity also suggests that the large surface area of graphene flakes could be one of the reasons for the enhancement of thermal conductivity of nano fluid.

Keywords: graphene, thermal conductivity, anti-wear, extreme pressure additive

INTRODUCTION

Improving the efficiency of coolants and lubricants has been an indispensable area of research for many decades. Several additives were introduced to enhance thermal and lubricating properties of the lubricants nevertheless the efficiency is still compromised. Recently, it was shown that the addition of nanometer sized (1-100 nm) particles to liquids could significantly enhance various properties of base fluids. Such nanoparticle suspensions are widely known as nanofluids or nanolubricants [1]. Nanofluids synthesised using various metallic, oxide, ceramic nanomaterials and even carbon nanotubes (CNT) exhibit excellent thermal conductivity [1-3], mass transfer [4], wetting spreading [5],antibacterial activity [6] and tribological properties. Thermal conductivity and viscosity are important physical properties of coolants/lubricants which are used to determine various design aspects of cooling systems including system geometry and dimensions, and pumping power. Several aspects pertaining to thermal conductivity and viscosity such as the effect of particle volume fraction, temperature dependence, particle size effect, base fluids, etc, have been studied in detail by many researchers [7-11]. A few reports have shown evidence of a relationship between the thermal and rheological behaviour of nanofluids [12, 13]. CNT nanofluids were

found superior to most of the metallic and oxide nanofluids [1, 12] in terms of enhanced thermal conductivity. Nonetheless, the discovery of graphene nano-flakes [14] made it possible to synthesize nanofluids with further enhanced thermal conductivity. Graphene nano-flakes are made of one layer of atomic carbon with theoretical specific surface area up to 2600 m^2/g [15]. In addition, it has excellent in-plane thermal conductivity which can be as high as 5200 W/m·k [16]. Graphene oxide nanosheets were found to enhance the thermal conductivity of water by up to 30.2% with volume fraction of 5.0% [17] and up to 47.5% with 0.25 wt.% [18]. Similarly, ethylene glycol based graphene nanofluids show an enhancement of 61.0 % with 5.0 % volume fraction [19]. The thermal conductivity of their functionalized-thermally exfoliated graphene (f-TEG) based nanofluids also showed an excellent enhancement up to ~60% at 50°C with a low volume fraction of 0.056% in deionized water [20]. An enhancement of 401.49% in viscosity of glycerol was achieved by loading of 2% graphene nanosheets at shear rate 6.32 s^{-1} and 20°C [21]. Few recent reports also discuss the effects of surfactants on graphene nanofluids stability [22], effect of surface modification of graphene [23], anti-wear effects [24], functionalization effect of graphene on overall properties [25] and Newtonian and non-Newtonian behaviors of graphene-water based nanofluids [26]. Although a few oil based suspensions have been investigated [25, 27], engine oil formulation with industrial standards have not been investigated extensively. In this study, we measured the thermal conductivity and viscosity of graphene based SAE20W50, API SN/CF and SJ/CF engine oil formulations. In addition we have also tested as- synthesized and functionalised graphene for stability in both water and mineral oil. The measured physical properties have been compared with values predicted by classical models as well as experimental data obtained from the literature. Moreover, the zeta potential was measured to study the stability of the suspensions.

EXPERIMENTAL DETAILS

Preparation, UV - Vis Spectrophotometry and SEM of Graphene nanofluids

Graphene nano-flakes of 60 nm average thickness and average particle (lateral) size ~ 3-7 µm having specific surface area <15 m^2/g was purchased from Graphene Labs Inc, USA. Graphene was functionalized using modified Hummer's method [28]. The graphene powder was suspended in mineral oil at 0.01 wt% concentration (Figure 1). Similarly stock solutions of various concentrations were prepared using as-synthesized graphene and functionalised graphene in both water and mineral oil. To ensure proper mixing of the nanoparticles in water, sonication was performed for 4 hours using bath-sonicator (JAC Sonicator 1505, 4 kHz). The samples were monitored to examine settling of nanoflakes. UV-Vis spectroscopy (Perkin-Elmer Lambda 35) was performed to confirm the characteristic peak of the samples.

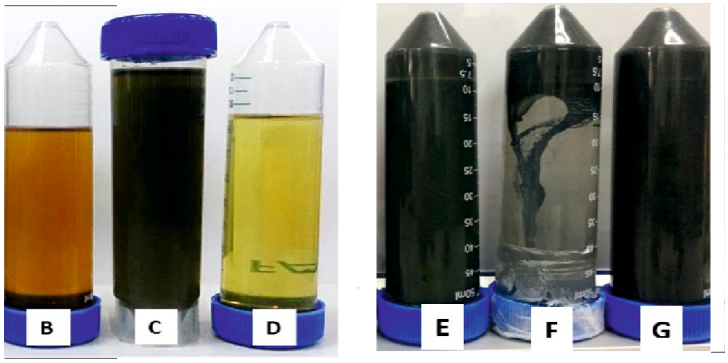

Figure 1. Engine oil samples (0.01wt%) representing stability. A – 20W50 SJ/CF+G60 nm; B1:20 dilution of A; C– 20W50 SN/CF+G60 nm; D-1:20 dilution of C; E, F G – Mineral oil of viscosity,150 SUS; 500 SUS; 2100 SUS respectively;

The graphene nanoflakes were mounted on stubs with conductive carbon tape and coated with-platinum using JEOL JFC-1600 auto fine coater. All samples were analyzed for their morphology and elemental compositions with energy-dispersive X-ray spectroscopy (EDX) using SEM (JOEL JSM 6400 LV, Japan).

Thermal conductivity and viscosity measurements

Thermal conductivity measurements of the graphene nanofluids were performed using a portable thermal conductivity meter KD2 Pro (Decagon Devices, Inc. USA). The transient line source (TLS) uses a sensor (single needle with 1.3 mm diameter and 60mm in length) to measure the thermal conductivity. A measurement cycle consists of 30 s of each equilibration, heating and cooling time. Standard glycerin was used for calibrating the device. The temperature measurements were made at the intervals of 1 s during both heating and cooling. Measurements are then fit with exponential integral functions using a non-linear least squares procedure. A linear drift term corrects for temperature changes of the sample during the measurement, to optimize the accuracy of the readings. To study the effect of temperature, a thermostat bath was used which maintained the temperature of the nanofluids. Nearly five readings were taken ateach temperature to ensure uncertainty in measurement with in ±5%.
The kinematic viscosity was measured using a Cannon-Fenske capillary viscometer. The measurements were carried out as per ASTM D440 standards. For reliability, the experiments were repeated at least thrice and at contolled conditions.

RESULTS AND DISCUSSION

Characterization

The characteristic spectra of graphene nanofluids (8 nm) were observed for concentrations such as 0.1, 0.06, 0.08 wt %. The absorbance was increasing with the increase in concentration andthe peak was observed approximately at 225 nm wavelength as shown in the Figure 2. This measurement is in good agreement with the existing reports.

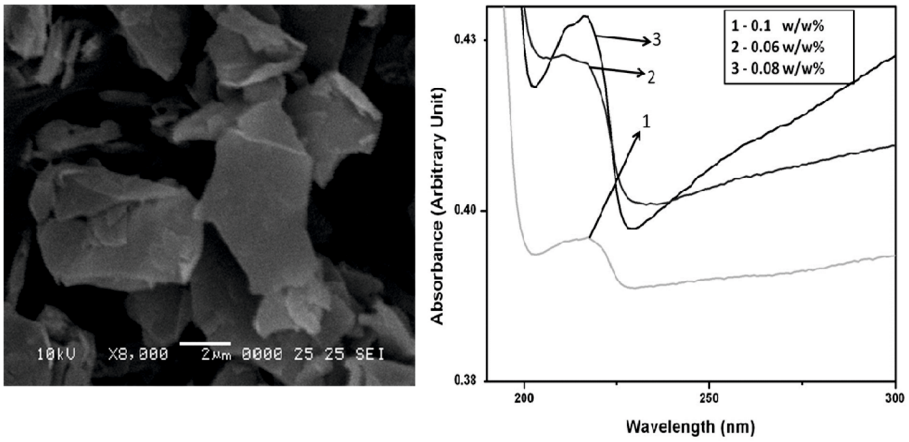

Figure 2. Left: Scanning electron microscope (SEM) image of 8 nm thickness from Graphene Labs Inc. USA; Right: UV-Vis spectra of graphene nanofluids. 1 - 0.1; 2 - 0.06; 3 – 0.08 w/w%;

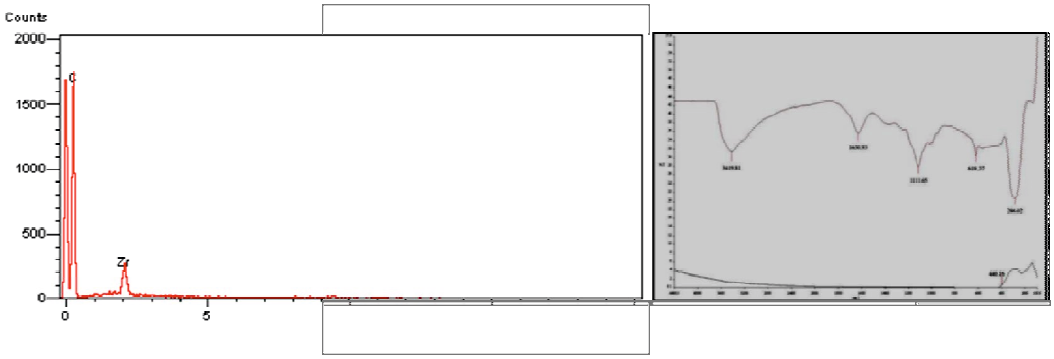

Figure 3. Left: EDX plot of Graphene nanoflakes; FTIR spectra of graphene;

Table 1: Attached Functional Groups of graphene 60 nm

Peaks	Attached Functional Groups - graphene 60 nm		
286.02	nil		
618.37	C-H bend acetylenic (alkynes)	C-Cl (acid chloride)	C-Cl stretch (alkyl halides)
1111.65	C-O Stretch (alcohol)	C-O-C (dialkyl-ethers)	C-C stretch (ketone)
1630.93	C-C (alkene)	C=O stretch (amides)	nil
3419.81	O-H stretch (alcohols)	O-H stretch (carboxylic acids)	nil

The SEM images with 2 μm magnification shows the physical nature of graphene flakes in powder form, Figure 2. The appearance of graphene shows that the flakes are single layered and stable without much agglomeration. The as-synthesized graphene is hydrophobic in nature and it does not disperse well in polar solvents. After EDX analysis, using quantitative method thegraphene flakes were analyzed and normalized results were obtained, Figure 3. The composition comprised of C - 92.89% and Zr – 7.11%. FTIR graphs shows the functional groups attached to graphene using acid functionalization.

Stability

Although the dispersion was not observed under a microscope, it is expected that the sonication would enable the graphene flakes to disperse uniformly. Zeta potential results in Table-1 show that that functionalized graphene in water and the as-synthesized graphene in the oil formulation is stable over a long period of time. Particle agglomeration, hydrophobicity, fluid polarity, surface charges of the particle and other factors determine the stability of the suspensions. According to DLVO theory, the sum of van der Waals attractive and electrical double layer (EDL) repulsive forces that exist between particles as they approach each other due to the Brownian motion determines the stability. Furthermore, the stability can be explained by
sedimentation ratio, from Stokes-Einstein theory (1897) [Eq. (1)], which is given by,

$$v = \frac{2r_p^2 \left| \rho_p - \rho_m \right| g}{9\varepsilon_m} \qquad (1)$$

where ρ_m = density of the medium, $\square_m$ = viscosity of the fluid, ρ_p = density of the particle, and r_p = radius of the nanoparticle. Lower the value of sedimentation ratio, higher the stability of the suspension. In case of water based stable suspension, the density of graphene is

comparable to the density of water and the sedimentation ratio is close to zero [29] resulting in the higher stability of the suspension. The pure base mineral oil as seen in the Figure 1 has poor stability owing to particle agglomeration and strong nonpolar nature.

Table 2. Zeta potential of oil samples

Basefluid	**Graphene concentration, wt%**	**Stability Improvement Method**	**Zeta Potential, mV**	**Stability Remarks**
H_2O	0.01 - 0.1	Acid Functionalization ofGraphene + Sonication	-70	Stable for more than 8 months
SAE 20W50 SN/CF	0.01 - 0.1	In-built Dispersants+ Sonication	1160	Stable over 1 month
SAE 20W50 SJ/CF	0.01 - 0.1	In-built Dispersants+ Sonication	714	Stable over 1 month
Base Oil 150 SUS	0.01 - 0.1	Sonication	18.4	Stable for 2 hrs
Base Oil 500 SUS	0.01 - 0.1	Sonication	22.1	Stable for 4 hrs

Thermal conductivity measurements

Figure 4 show that concentration of graphene as low as 0.01 wt% could enhance the thermal conductivity of engine oil (SAE 20W50 SN/CF) upto 22.3% at 80 °C. The SAE 20W50 SJ/CF has 5.4% low enhancement than SN/CF oil formulation. The thermal conductivity was found to be the function of nanoparticle concentration however, after a particular concentration (>0.1wt%) the conductivity doesn't enhance further. It might be due to the agglomeration of nanoparticles at higher concentrations due to van der Waals forces of attraction, restricting its Brownian motion (both rotational and translational motions) [30].

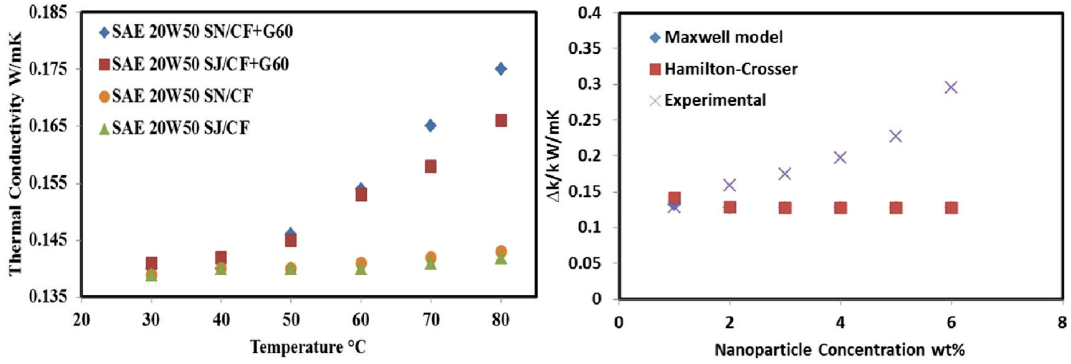

Figure 4. Thermal conductivity with respect to temperature of mineral oil formulation with and without 0.01wt% graphene (60 nm)

Furthermore, it was observed that the oil formulation which contains various inbuilt dispersants help graphene to remain stable whereas, the stability of pure base oil decreases due to poor dispersion without dispersants (Figure 1). Hence the thermal conductivity of stable oil formulation is better than that of pure base oil containing graphene with identical concentration. The thermal conductivity results of graphene-oil formulation was compared with Maxwell and Hamilton-Crosser models (Figure 4). Thermal conductivity using Maxwell's equation (2) relies on the volume fraction, spherical shape of particle and base fluid thermal condu tivity;

$$k_{eff} = \frac{k_p + 2k_b + 2\left(k_p - k_b\right)\phi}{k_p + 2k_b - \left(k_p - k_b\right)\phi} k_b \tag{2}$$

where k_p is thermal conductivity of nanoparticle, k_f is thermal conductivity of base fluid and ϕ is the volume fraction. Hamilton-Crosser model (equation 3) is a modification of Maxwell's model which is applicable to non-spherical particles,

$$k_{eff} = \frac{k_p + (n-1)k_f - (n-1)\phi(k_f - k_p)}{k_p + (n-1)k_f + \phi(k_f - k_p)} k_f \tag{3}$$

where k_p is thermal conductivity of nanoparticle, k_f is thermal conductivity of base fluid, $k_p/k_f > 100$, n is an empirical shape factor $n = \frac{2}{\Psi}$ and Ψ is the sphericity. Interestingly, we observed that at low temperature range (25 - 45 °C) thermal conductivity values from Maxwell model is close to the experimental results and the results from H-C model are slightly higher. However, in some studies, it was found that even at low concentration the measured thermal conductivity of nanofluids is greater than that predicted by classical models [31-33]. This is due to the fact that these models were developed for milli or micro sized particles as discontinuous phase. In addition they do not account for particle geometry, temperature effect, Brownian motion of nanoparticles, the effect of interfacial layer at particle/liquid interface, and the effect of nanoparticles clustering, which are considered as important mechanisms for enhancing the thermal conductivity of nanofluids [2, 34-37]. However, some reports found Nan's model [38] to be closely predicting k_{eff} and it exprecesses the resulting effective thermal conductivity of the composite for completely misoriented ellipsoidal particles as,

$$k = k_0 \frac{3 + \varphi[2\beta_{11}(1 - L_{11}) + \beta_{33}(1 - L_{33})]}{3 - \varphi(2\beta_{11} L_{11} + \beta_{33} L_{33})} \tag{4}$$

$$\text{where } \beta_{ii} = \frac{k_p - k_0}{k_0 + L_{11}(k_p - k_0)} \tag{5}$$

where L_{11} and φ are the geometrical factors and the volume fraction of particles, respectively. k_p is the thermal conductivity of the ellipsoidal particles. For graphene and graphene oxide, the aspect ratio is very high, so L11=0 and L33=1.

Existing reports show that the temperature has a significant effect on enhanced thermal conductivity of nanofluids [37, 39, 40]. Graphene oxide nanosheets were found to enhance the thermal conductivity of water by up to 30.2% when suspended at 5.0 vol%. Similarly, ethylene glycol based nanofluids show an enhancement of 61.0 % with 5.0 vol% volume fraction. Most nanofluids exhibit particle volume fraction and temperature dependent thermal conductivity [1, 2, 37]. However, recent works indicate that the enhancement ratios of the graphene nanofluidsare nearly constant with varying temperature, and they are reduced with increasing thermal conductivity of the base fluids. Another work appears to suggest that the thermal conductivity of functionalized and thermally exfoliated of graphene (f-TEG) based nanofluids is temperature dependent [20]. The thermal conductivity of f-TEG based nanofluids showed an excellent enhancement up to ~60% at 50°C with a volume fraction of 0.056% in deionized water [20]. Thepresent experimental results confirm that the thermal conductivity of graphene nanofluids is strongly temperature and nanoflakes concentration dependent (Figure 4). The reasons for this enhancement can be attributed to graphene's large surface area [41, 42], dispersion of nanoflakes
[43] and Brownian motion of GNFs. It is well known from the early reports on nanofluids that the inherently stochastic motion of nanoparticles could be a probable explanation for the thermal conductivity enhancement since smaller particles show greater enhancements of thermal conductivity with temperature than do larger particles [37, 44]. Similarly, elevated temperature might modulate random motion of GNFs in fluid and thus resulting in considerable enhancement of thermal conductivity.

Viscosity of graphene nanofluids

Viscosity is one the important properties of nanofluids which governs its flow behaviour in various applications. Few research groups examined the viscosity of various nanofluids

including oxide [45, 46] and carbon nanotubes [13, 47]. In this study, kinematic viscosity and dynamic viscosity of graphene-oil suspension has been investigated.

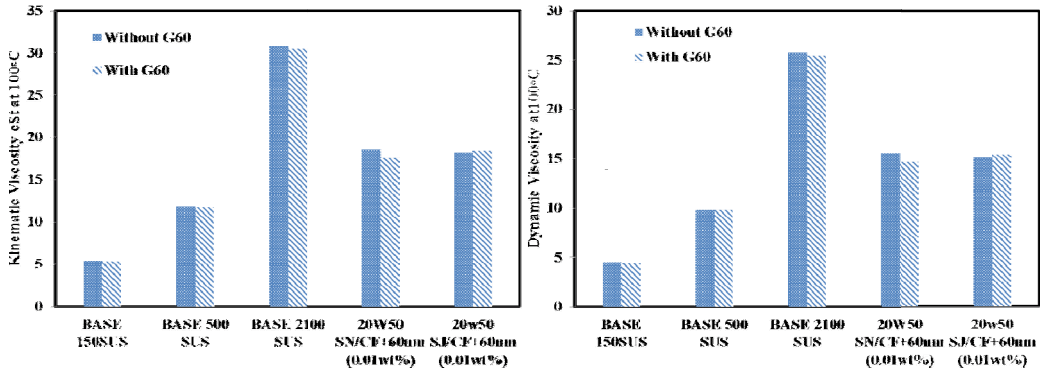

Figure 5. Kinematic Viscosity; Left: Effect of temperature using two sizes of graphene (60 and 12 nm); Right: Various base fluids using 60 nm graphene;

The measured kinematic viscosity of the nanolubricant has negligible difference than the base oil. Dynamic viscosity was calculated using the density of base oil which also shows negligible difference. Several reports have compared the experimental values against the Einstein's model which predicts the effective viscosity of a fluid according to the following equation,

$$\mu_{eff} = \mu_b (1 + 2.5\phi) \tag{1}$$

where μ_b is the viscosity of base fluid and ϕ is the volume fraction. The temperature dependent viscosity can be calculated from equation (5) provided that the viscosity of the base fluid at the corresponding temperature is known. Few classical models [33, 48, 49] used the differential effective medium approach for spherical particle suspensions to extend the Einstein's formula for a moderate particle volume fraction. However, exact prediction of viscos ty for graphene

nanofluids using these classical models is not possible. Based on Mooney (1951) model, another expression was developed for non-spherical particles [50, 51] as,

$$\ln\left(\frac{\mu}{\mu_f}\right) = \frac{\mu_\infty \phi}{1 - \phi/\phi_m} \tag{2}$$

where □ the volume fraction and ϕ_m is the maximum packing volume fraction. This model can be use to predict the viscosity of graphene flakes based nanofluids which are similar to plate-like Ba-Ferrite. Using $\phi_m = 0.65$, the expression (6) fitted very well with their measured viscosities for plate-like Ba–Ferrite particle for volume fraction up to 0.04. From this expression the intrinsic viscosity at infinite shear rate was also evaluated where $\mu_\infty = 12$ cP for plate-like Ba–Ferrite particle. Nevertheless, in the present studies, the experiements were limited to single concentration of graphene at 40 and 100°C, and therefore the models could not be used.

Effect of temperature on viscosity

Nguyen et al. (2008) experimentally investigated the effect of temperature and particle volume concentration on the dynamic viscosity of water based Al_2O_3 nanofluids. They found that the dynamic viscosity of nanofluids increases considerably with particle volume fraction but clearly decreases with a temperature increase [53]. In addition, it was observed that a critical temperature exists beyond which the particle suspension properties seem to be drastically altered,triggering a hysteresis phenomenon. This critical temperature is found to be strongly dependent of both particle concentration and size. Furthermore, another research group found that the viscosity of water based TiO_2 nanofluids to be decreasing along increasing temperature [54].

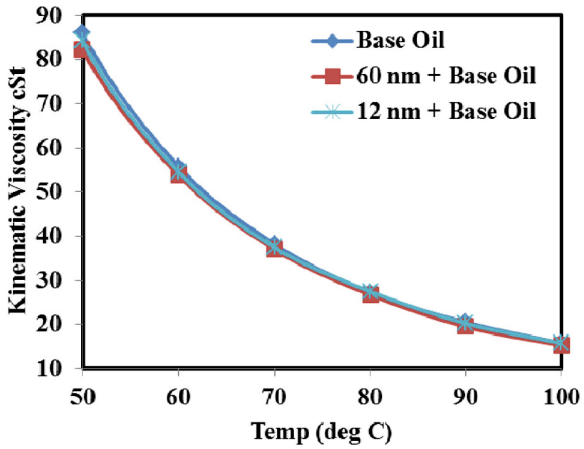

Figure 6. Kinematic viscosity of graphene based oil formuation with respect to temperature

Figure 6 shows that the viscosity of our graphene nanofluids significantly reduces with temperature. The viscosity drops intensely from 60 to 40°C. It might be due to increased Brownian diffusion at elevated temperatures. Whereas below 40°C the Brownian diffusion might be weak owing to higher base-fluid viscosity. At very high-shear rates, the Brownian diffusion plays a negligible role in comparison with the convective contribution and hence independent of the high-shear viscosity on the temperature.

CONCLUSION

We synthesized graphene-oil nanofluids using as-synthesised graphene nanoflakes. Graphene nanoflakes were characterized by SEM, UV-Vis and EDX. We measured physical properties affecting the performance of graphene nanofluids as lubricants/ oolants; namely thermal conductivity and viscosity. The effects of the particle volume fraction and temperature on the thermal conductivity and viscosity were investigated. Observations showed that the thermal conductivity of oil formulation could be enhanced by 22.3% by adding 0.01wt% graphene. The results were compared with the models of Maxwell and Hamilton-Crosser, where

these models were able to predict the thermal conductivity enhancement of graphene nanofluids. When experimented for viscosity, the graphene-oil suspension showed almost no changes in viscosity with the addition of graphene.

NOMENCLATURE

k_{eff}	effective thermal conductivity, $Wm^{-1}K^{-1}$
k_p	thermal conductivity of nanoparticles, $Wm^{-1}K^{-1}$
k_b	thermal conductivity of base fluid, $Wm^{-1}K^{-1}$
n	empirical shape factor ($n = \frac{2}{\Psi}$)
k_c	thermal conductivity of the CNTs, $Wm^{-1}K^{-1}$
L	length of CNT, nm
d	diameter of CNT, nm
R_k	thermal resistance of the nanotube-fluid interface
T_0	reference value
g	acceleration of gravity
Δh	upstream hydrostatic head minus downstream hydrostatic head
ν	kinematic viscosity
ΔP	total up-stream pressure minus total downstream pressure
R	capillary radius
L	capillary length
μ	absolute viscosity
□	particle volume fraction
ξ	constant
ψ	sphericity
μ_{eff}	effective viscosity of nanofluids
μ_f	effective viscosity of base fluid
μ_∞	intrinsic viscosity at infinite shear rate
μ_0	reference value
$□_m$	maximum packing volume fraction
eff	effective
p	nanoparticles
b	basefluid
c	CNT
∞	infinity

References

1. Choi, S.U.S., et al., *Anomalous thermal conductivity enhancement in nanotube suspensions.* Applied Physics Letters, 2001. **79**(14): p. 2252-2254.

2. Eastman, J.A., et al., *Anomalously increased effective thermal conductivities of ethylene glycol-based nanofluids containing copper nanoparticles.* Applied Physics Letters, 2001. **78**(6): p. 718-720.

3. Xie, H., et al., *Thermal conductivity enhancement of suspensions containing nanosized alumina particles.* Journal of Applied Physics, 2002. **91**(7): p. 4568-4572.

4. Krishnamurthy, S., et al., *Enhanced Mass Transport in Nanofluids.* Nano Letters, 2006. **6**(3): p. 419-423.

5. Kondiparty, K., et al., *Wetting and Spreading of Nanofluids on Solid Surfaces Driven by the Structural Disjoining Pressure: Statics Analysis and Experiments.* Langmuir, 2003. **27**(7): p. 3324-3335.

6. Zhang, L., et al., *Investigation into the antibacterial behaviour of suspensions of ZnO nanoparticles (ZnO nanofluids).* Journal of Nanoparticle Research, 2007. **9**(3): p. 479- 489.

7. Buongiorno, J., et al., *A benchmark study on the thermal conductivity of nanofluids.* Journal of Applied Physics, 2009. **106**(9): p. 094312-14.

8. Özerinç, S., S. Kakaç, and A. Yaz□□oğlu, *Enhanced thermal conductivity of nanofluids: a state-of-the-art review.* Microfluidics and Nanofluidics, 2010. **8**(2): p. 145-170.

9. Fan, J. and L. Wang, *Review of Heat Conduction in Nanofluids.* Journal of Heat Transfer, 2011. **133**(4): p. 040801-14.

10. Thomas, S. and B.P.S. Choondal, *A review of experimental investigations on thermal phenomena in nanofluids.* Nanoscale Research Letters, 2011. **6**(377).

11. Yu, W. and H. Xie, *A Review on Nanofluids: Preparation, Stability Mechanisms, and Applications.* Journal of Nanomaterials, 2012. **2012**.

12. Ding, Y., et al., *Heat transfer of aqueous suspensions of carbon nanotubes (CNT nanofluids).* International Journal of Heat and Mass Transfer, 2006. **49**(1-2): p. 240-250.

13. Yang, Y., *Thermal and rheological properties of carbon nanotube-in-oil dispersions.* J. Appl. Phys., 2006. **99**(11): p. 114307.

14. Novoselov, K.S., et al., *Electric Field Effect in Atomically Thin Carbon Films.* Science, 2004. **306**(5696): p. 666-669.

15. Chae, H.K., et al., *A route to high surface area, porosity and inclusion of large molecules in crystals.* Nature, 2004. **427**(6974): p. 523-527.

16. Balandin, A.A., et al., *Superior Thermal Conductivity of Single-Layer Graphene.* Nano Letters, 2008. **8**(3): p. 902-907.

17. Yu, W., H. Xie, and D. Bao, *Enhanced thermal conductivities of nanofluids containing graphene oxide nanosheets.* Nanotechnology, 2010A. **21**.

18. Hajjar, Z., A.m. Rashidi, and A. Ghozatloo, *Enhanced thermal conductivities of graphene oxide nanofluids.* International Communications in Heat and Mass Transfer, 2014. **57**(0): p. 128-131.

19. Yu, W., H. Xie, and W. Chen, *Experimental investigation on thermal conductivity of nanofluids containing graphene oxide nanosheets.* Journal of Applied Physics, 2010B. **107**(9): p. 094317-6.

20. Baby, T.T. and S. Ramaprabhu, *Investigation of thermal and electrical conductivity of graphene based nanofluids.* Journal of Applied Physics, 2010. **108**(12): p. 124308-6.

21. Moghaddam, M.B., et al., *Preparation, characterization, and rheological properties of graphene–glycerol nanofluids.* Chemical Engineering Journal, 2013. **231**(0): p. 365-372.

22. Uddin, M.E., et al., *Effects of various surfactants on the dispersion stability and electrical conductivity of surface modified graphene.* Journal of Alloys and Compounds, 2013. **562**(0): p. 134-142.

23. Li, X., et al., *Effect of surface modification on the stability and thermal conductivity of water-based SiO2-coated graphene nanofluid.* Thermochimica Acta, 2014. **595**(0): p. 6-10.

24. Taha-Tijerina, J., et al., *Multifunctional nanofluids with 2D nanosheets for thermal and tribological management.* Wear, 2013. **302**(1–2): p. 1241-1248.

25. Ma, W., et al., *Silicone based nanofluids containing functionalized graphene nanosheets.* Colloids and Surfaces A: Physicochemical and Engineering Aspects, 2013. **431**(0): p. 120-126.

26. Mehrali, M., et al., *Investigation of thermal conductivity and rheological properties of nanofluids containing graphene nanoplatelets.* Nanoscale Research Letters, 2014. **9**(1): p. 15.

27. Eswaraiah, V., V. Sankaranarayanan, and S. Ramaprabhu, *Graphene-Based Engine Oil Nanofluids for Tribological Applications.* ACS Applied Materials & Interfaces, 2011. **3**(11): p. 4221-4227.

28. Hummers, W.S. and R.E. Offeman, *Preparation of Graphitic Oxide.* Journal of theAmerican Chemical Society, 1958. **80**(6): p. 1339-1339.

29. Sen Gupta, S., et al., *Thermal conductivity enhancement of nanofluids containing graphene nanosheets.* Journal of Applied Physics, 2011. **110**(8): p. -.

30. Timofeeva, E.V., J.L. Routbort, and D. Singh, *Particle shape effects on thermophysical properties of alumina nanofluids.* Journal of Applied Physics, 2009. **106**(1): p. -.

31. Maxwell, J.C., *A Treatise on Electricity and Magnetism.* Oxford: Clarendon, 1892. **2**(3): p. 68-73.

32. Hamilton, R.L. and O.K. Crosser, *Thermal Conductivity of Heterogeneous Two- Component Systems.* Industrial & Engineering Chemistry Fundamentals, 1962. **1**: p. 187- 191.

33. Bruggeman, D.A.G., *Berechnung verschiedener physikalisher Konstanten von heterogenen Substanzen: I. Dielektrizit¨ atskonstanten und Leitf¨ ahigkeiten der Mischk¨orper aus isotropen Substanzen.* Annalen der Physik, 1935. **24**: p. 636-664.

34. Lee, S., et al., *Measuring Thermal Conductivity of Fluids Containing Oxide Nanoparticles.* Journal of Heat Transfer, 1999. **121**(2): p. 280-289.

35. Keblinski, P., et al., *Mechanisms of heat flow in suspensions of nano-sized particles (nanofluids).* International Journal of Heat and Mass Transfer, 2002. **45**(4): p. 855-863.

36. Xue, L., et al., *Effect of liquid layering at the liquid-solid interface on thermal transport.* International Journal of Heat and Mass Transfer, 2004. **47**(19-20): p. 4277-4284.

37. Das, S.K., P.N.T. P., and W. Roetzel, *Temperature dependence of thermal conductivity enhancement for nanofluids.* J. Heat Transfer, 2003. **125**(4): p. 567.

38. Nan, C.-W., et al., *Effective thermal conductivity of particulate composites with interfacial thermal resistance.* Journal of Applied Physics, 1997. **81**(10): p. 6692-6699.

39. Chon, C.H., et al., *Empirical correlation finding the role of temperature and particle size for nanofluid (Al2O3) thermal conductivity enhancement.* Appl. Phys. Lett., 2005. **87**: p. 3.

40. Li, C.H., *Experimental investigation of temperature and volume fraction variations on the effective thermal conductivity of nanoparticle suspensions (nanofluids).* J. Appl. Phys., 2006. **99**(8): p. 084314.

41. Beck, M., et al., *The effect of particle size on the thermal conductivity of aluminananofluids.* Journal of Nanoparticle Research, 2009. **11**(5): p. 1129-1136.

42. Kim, S.H., S.R. Choi, and D. Kim, *Thermal Conductivity of Metal-Oxide Nanofluids: Particle Size Dependence and Effect of Laser Irradiation.* Journal of Heat Transfer, 2007. **129**(3): p. 298-307.

43. Katsnelson, M.I. and K.S. Novoselov, *Graphene: New bridge between condensed matter physics and quantum electrodynamics.* Solid State Communications, 2007. **143**(1-2): p. 3-13.

44. Jang, S.P. and S.U.S. Choi, *Role of Brownian motion in the enhanced thermal conductivity of nanofluids.* Applied Physics Letters, 2004. **84**(21): p. 4316-4318.

45. Anoop, K.B., et al., *Rheological and flow characteristics of nanofluids: Influence of electroviscous effects and particle agglomeration.* Journal of Applied Physics, 2009. **106**(3).

46. Duangthongsuk, W. and S. Wongwises, *Measurement of temperature-dependent thermal conductivity and viscosity of TiO2-water nanofluids.* Experimental Thermal and Fluid Science, 2009. **33**(4): p. 706-714.

47. Garg, P., et al., *An experimental study on the effect of ultrasonication on viscosity and heat transfer performance of multi-wall carbon nanotube-based aqueous nanofluids.* International Journal of Heat and Mass Transfer, 2009. **52**(21-22): p. 5090-5101.

48. Brinkman, H.C., *The Viscosity of Concentrated Suspensions and Solutions.* The Journal of Chemical Physics, 1952. **20**(4): p. 571-571.

49. Mooney, M., *The viscosity of a concentrated suspension of spherical particles.* Journal of Colloid Science, 1951. **6**(2): p. 162-170.

50. Choi, H.J., T.M. Kwon, and M.S. Jhon, *Effects of shear rate and particle concentration on rheological properties of magnetic particle suspensions.* Journal of Materials Science, 2000. **35**(4): p. 889-894.

51. Kwon, T.M., M.S. Jhon, and H.J. Choi, *Viscosity of magnetic particle suspension.* Journal of Molecular Liquids, 1998. **75**(2): p. 115-126.

52. Renner, J.r., B. Evans, and G. Hirth, *On the rheologically critical melt fraction.* Earth and Planetary Science Letters, 2000. **181**(4): p. 585-594.

53. Nguyen, C.T., et al., *Viscosity data for Al_2O_3-water nanofluid-hysteresis: is heat transfer enhancement using nanofluids reliable?* International Journal of Thermal Sciences, 2008. **47**(2): p. 103-111.

54. Murshed, S.M.S., K.C. Leong, and C. Yang, *Investigations of thermal conductivity and viscosity of nanofluids.* International Journal of Thermal Sciences, 2008. **47**(5): p. 560-568.